Optimization of ECMAP Parameters in the Production of Ultra-Fine Grained Al1050 Strips Using Grey Relational Analysis

Peyman Mashhadi Keshtiban[1,*], Mohammad Zadshakouyan[1], Ghader Faraji[2]

[1]Department of Mechanical Engineering, University of Tabriz, Tabriz, Iran
[2]Department of Mechanical Engineering, College of Engineering, University of Tehran, Tehran 11155-4563, Iran

ARTICLE INFO

Article history:
Received 2 September 2015
Accepted 2 November 2015
Available online 20 January 2015

Keywords:
Equal channel multi angular pressing
Strip, Optimization
Finite element

ABSTRACT

Production of lightweight metals with a higher strength to weight ratio is always the main goal of researchers. In this article, the equal channel multi angular pressing (ECMAP) process as one of the most appealing severe plastic deformation (SPD) methods for production of ultra-fine grained (UFG) materials is studied. Two main routes A and C were investigated by finite element method (FEM) and compared with each other from different perspectives. ABAQUS commercial software was used to evaluate the maximum strain, maximum required force, and strain inhomogeneity index in both routes and the obtained FEM results were verified by both theoretical calculations and experimental tests. It is inferred that although equivalent plastic strain (PEEQ) in route A is higher than that in route C, the strain homogeneity as a quality factor for route C is higher. So, route C was selected for more investigation and optimization. Grey relational analysis was used as the optimization method. Geometrical parameters were taken as input variables and both inhomogeneity index and maximum required load were taken as objectives. Then, the suggested tests by full factorial method were simulated by FEM. After optimization, it was concluded that the best set up belongs to experiment number 20 in which the values of Φ_1, ψ_1 and ψ_2 are 165°, 0° and 15°, respectively. Also, it was inferred that among geometrical parameters, die channel angle (Φ_1) is the most effective parameter.

1. Introduction

Nowadays, materials with ultra-fine grained structure have got a rising interest of the researchers. Hall-Petch equation demonstrates that the materials with smaller grain size show more strength.

$$\sigma_y = \sigma_0 + K_y d^{-1/2} \quad (1)$$

where d is the grain diameter of average size, σ_y is the yield stress, σ_0 is the reference yield stress, and K_y is the yield constant [1]. Besides improving mechanical properties, SPD methods do not have negative effects like reducing weldability and formability [2]. The ECAP process as one of the most efficient types of SPD methods has often been concentrated on and researched. So, ECAP was studied precisely in various ways. Some studies focused on experimental works and observations [3-8]. Different pure metals and a range of industrial metal alloys deformed severely and comparison was done before and after ECAP on the variation of microstructure or mechanical behavior. In order to enhance the process efficiency and decrease the expense of trial and error, some other researchers simulated the process by FEM, and validated the results by experimental works [9-14]. Different softwares were used in these works

* Corresponding Author:
E-mail Address: pmkmech@gmail.com

and different FEM simulations in 2D or 3D spaces were done.

The majority of works done on circular or square cross section and strip type pieces with rectangular cross section were hardly discussed in previous ECAP works [15, 16]. Because of some technical limitations, researchers usually focused on one pass mold and tested one pass ECAP or multi pass ECAP with the subjected die. So, few articles were published about ECMAP [17-24]. Nakashima et al. [17], Kim [18], and Jung et al. [19] developed the ECMAP of samples with square cross sections. Recently, Faraji et al. suggested two pass [20, 21] and three pass [22-24] mold as multi pass tubular channel angular pressing (TCAP) for producing nanostructured tubes. Furthermore, optimization methods were rarely applied to the ECAP process and researchers usually did optimization by expensive and time consuming experimental works [25-29]. In an innovative study, Chengpeng et al. [30] applied grey theory for structural optimization of just one pass ECAP with elliptical cross section. However, multi objective optimization of ECMAP parameters on strip type products has never been studied before.

In this article, the ECMAP process as one of the most appealing SPD methods for the production of ultra-fine grained (UFG) Al1050 strips is studied. Two main routes A and C are investigated by FEM and compared with each other from different points of the view. Route C with more positive results is selected for further investigation and optimization. Grey relational analysis is used as the optimization method. Geometrical parameters are taken as input variables and both inhomogeneity index and maximum required load are taken as objectives. Results are validated by analytical methods and experimental tests. Then for all input and output parameters, optimization is done and optimum values of the input parameters and also the effectiveness of each parameter are obtained.

2. Finite element, experimental and optimization procedures

2.1. Finite element and experimental procedures

Numerical simulations were done by Abaqus/ Explicit commercial finite element code. In the strip type specimen, there is not any strain in width direction; so, plane strain model was used. The element type is 4-node bilinear plane strain quadrilateral, reduced integration, hourglass control (CPE4R). To apply large strains during simulation, the adaptive mesh was used by considering the Arbitrary Lagrangian Eulerian (ALE) method. In the ALE formulation, the FE mesh is neither attached to the material nor fixed in space. Moreover, the concentration of the mesh in a particular region and the mesh distortion are controlled by a procedure. Therefore, it is possible to manage the path-dependent behavior of the material and the free surface conditions while maintaining the mesh suitability by using the ALE formulation [31]. Penalty method and Columb friction condition were considered between the contacting surfaces and the friction coefficient was taken to be 0.1 [19, 32]. Die and punch were taken as rigid analytical bodies.

Die Geometrical parameters for both routes A & C are depicted in Fig.1 (a) and (b), correspondingly. The geometry of designated die revealed that three equal channel angular pressing occur on each element of the ECMAPed strips. Because of the symmetry in entrance and exit channels, four parameters exist in die (Φ_1, Φ_2, $\psi_1$and ψ_2). Schematic of ECMAP and experimental setup of designed die are shown in Fig. 2 (a) and (b), respectively.

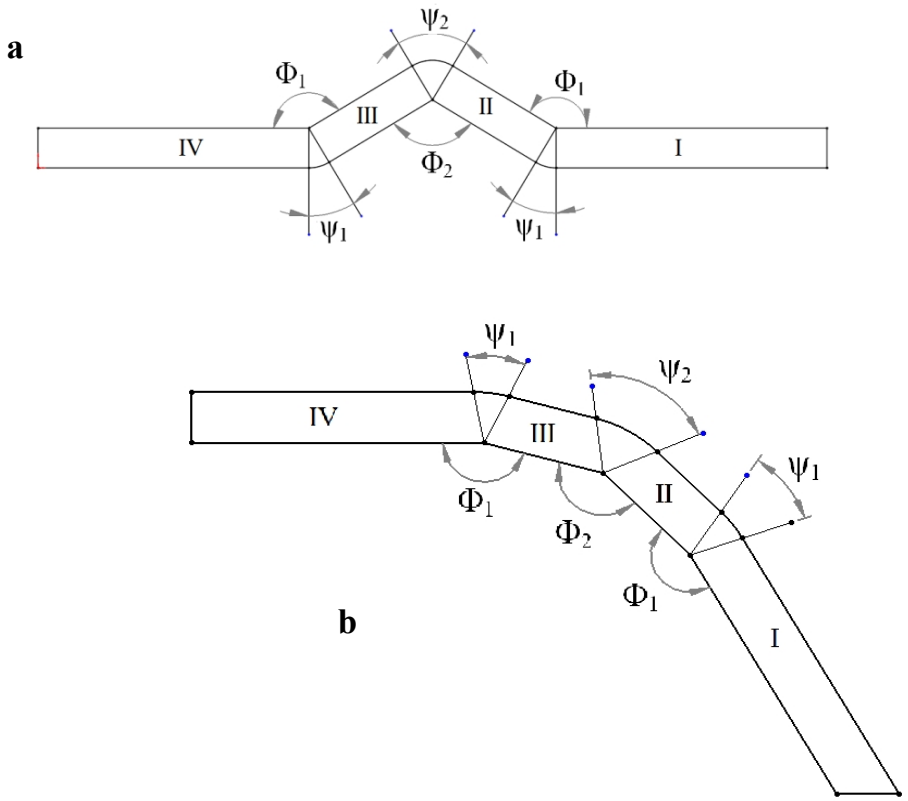

Fig 1. The process parameters for (a) route C and (b) route A

After the quantometric test, the Al1050 composition was obtained and the results are listed in Table 1. After the tensile test, mechanical properties of Al1050 were listed in Table 2. Strip samples of 20 mm × 60 mm were cut from a sheet of 3 mm thickness. The die was manufactured from CK60 steel and hardened to reach 60 RC hardness. For better force control and easier splitting die halves, the outer surface was preferred to be in the shape of a truncated cone. For accurate assembling of die parts, six grinded pins were positioned in the farthest places on die halves (Fig. 2). For each considered value of Φ_1, the dependent parameter (Φ_2) can be calculated from Eq. (2) which is the triangle equation obtained from the triangle created in middle part of route C.

Table 1. Composition of Al1050

Si	Fe	Cu	Mn	Mg	Zn	Ti
0.10154	0.25277	0.00672	0.04187	0.01537	0.02269	0.04327
Cr	Ni	Pb	Sn	V	Sb	Al
0.00120	0.00406	0.00828	0.00001	0.01198	0.00967	99.4999

Table 2. Mechanical properties of Al1050

Parameter	Value
Young's modulus (E)	69GPa
Poisson's ration (ν)	0.33
Density (ρ)	2700 kg/m^3
Thickness (t)	3mm

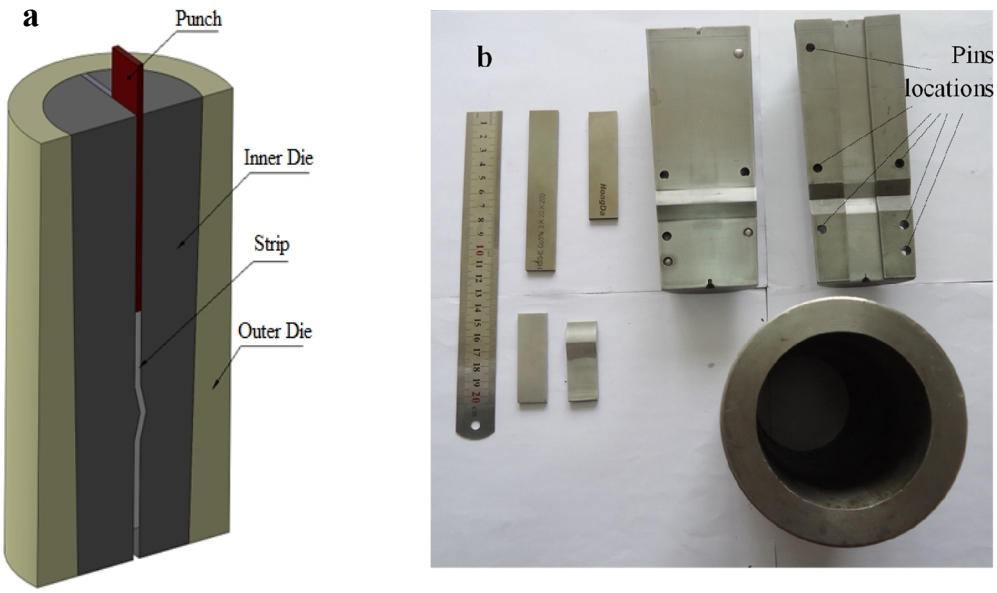

Fig 2. The designed die: (a) schematic of ECMAP and (b) experimental setup

$$\Phi_2 = 2\,\Phi_1 - \pi \quad (2)$$

Two other parameters $\psi_1$and ψ_2 are dependent parameters and should be chosen from the specified zone [1]:

$$0 < \psi_1 < \pi - \Phi_1 \ , \quad 0 < \psi_2 < \pi - \Phi_2 \quad (3)$$

The parameters Φ_1, $\psi_1$and ψ_2 were taken to be 165°, 15° and 30°, respectively. These values belong to set number 27 of the suggested factorial design tests.

2.2. Optimization

2.2.1 Factorial design

The input parameters for optimization were taken to be Φ_1, $\psi_1$and ψ_2, and listed in Table 3. Φ_2 is the dependent variable achieved from Eq. (2). Also, the maximum and minimum values of ψ_i should be in a special range (Eq. 3). For each selected Φ_1, three levels of ψ_i were considered starting from minimum to a maximum amount. Then the suggested tests were simulated by FEM and both inhomogeneity index and maximum required load were attained as objectives (Table 4).

Table 3. Geometrical parameters and levels

Parameter	Level								
Φ_1	145			155			165		
ψ_1	0	17.5	35	0	12.5	25	0	7.5	15
ψ_2	0	35	70	0	25	50	0	15	30

Table 4. Input and output variables

	Φ_1	ψ_1	ψ_2	Maximum required load	Inhomogeneity index
1		0	0	10166.3	0.187
2		0	35	9262.88	0.200
3		0	70	9650.81	0.050
4		17.5	0	10640.8	0.243
5	145	17.5	35	10444.4	0.202
6		17.5	70	10979.8	0.088
7		35	0	11330.5	0.218
8		35	35	10979.8	0.184
9		35	70	10856.7	0.034

	Φ_1	ψ_1	ψ_2	Maximum required load	Inhomogeneity index
10		0	0	5097.32	0.197
11		0	25	4320.08	0.071
12		0	50	4973.7	0.117
13		12.5	0	4097.81	0.122
14	155	12.5	25	4405.83	0.080
15		12.5	50	4986.06	0.105
16		25	0	5089.53	0.149
17		25	25	4484.96	0.052
18		25	50	4746.27	0.139
19		0	0	1910.24	0.184
20		0	15	1899.8	0.181
21		0	30	1919.07	0.310
22		7.5	0	1854.17	0.213
23	165	7.5	15	1861.78	0.234
24		7.5	30	2142.72	0.293
25		15	0	1865.03	0.256
26		15	15	1988.47	0.233
27		15	30	2062.91	0.250

2.2.2 Grey relational analysis

The objective parameters should be normalized firstly so that grey relational coefficient and grey relational grade can be calculated subsequently. Finally, to find the best values of parameters, the grey relational graph was plotted.

2.2.3 Grey relational generation

To make correct comparison, all the influencing parameters were changed to be in the same range. So, for comparison viability, the parameters should be normalized. Based on the type of optimization, normalizing of parameters will be done by one of the equations from (4) to (6) [33].

For objective parameters:

when the objective is the minimum value, Eq. (4),

$$X_i^*(k) = 1 - \frac{\max X_i^0(k) - X_i^0(k)}{\max X_i^0(k) - \min X_i^0(k)} \quad (4)$$

when the objective is the preferred value, Eq. (5),

$$X_i^*(k) = 1 - \frac{\left| X_i^0(k) - X^0 \right|}{\max X_i^0(k) - X^0} \quad (5)$$

and when the objective is the maximum value, Eq. (6) will be used.

$$X_i^*(k) = 1 - \frac{X_i^0(k) - \min X_i^0(k)}{\max X_i^0(k) - \min X_i^0(k)} \quad (6)$$

Where $X_i^*(k)$ is the value of the parameter after generation, X^0 is the preferred value, $\max X_i^0(k)$ and $\min X_i^0(k)$ denote the maximum and minimum value of $X_i^0(k)$ respectively [34]. In this study, the optimum condition for both strain inhomogeneity index and maximum required load occurs in minimum value so, Eq. (4) was employed.

2.2.4 Grey relational coefficient

Grey relational coefficient was calculated for each objective parameter by Eq. (7) and listed in Table 5. This coefficient is the number between zero and one. For each objective parameter, grey relational coefficient demonstrates the amount of closeness from optimum value [35, 36].

Table 5. Grey relational coefficient and grey relational grade

Simulation no.	Grey relational coefficient		Grey relational grade	Orders
	Maximum required load	Inhomogeneity index		
1	0.534	0.406	0.470	16
2	1.000	0.386	0.693	11
3	0.727	0.867	0.797	4
4	0.429	0.333	0.381	24
5	0.467	0.383	0.425	21
6	0.376	0.659	0.518	14
7	0.333	0.362	0.348	26
8	0.376	0.411	0.393	22
9	0.393	1.000	0.697	9
10	0.333	0.333	0.333	27
11	0.692	0.792	0.742	8
12	0.363	0.527	0.445	19
13	1.000	0.509	0.754	6
14	0.619	0.721	0.670	12
15	0.360	0.578	0.469	17
16	0.335	0.428	0.381	23
17	0.563	1.000	0.782	5
18	0.435	0.455	0.445	20
19	0.720	0.956	0.838	2
20	0.760	1.000	0.880	1
21	0.690	0.333	0.512	15
22	1.000	0.668	0.834	3
23	0.950	0.549	0.749	7
24	0.333	0.365	0.349	25
25	0.930	0.462	0.696	10
26	0.518	0.554	0.536	13
27	0.409	0.483	0.446	18

$$\xi_i(k) = \frac{\Delta_{\min} + \xi\Delta_{\max}}{\Delta_{0i}(k) + \xi\Delta_{\max}} \quad (7)$$

where $\Delta_{\min}$ and $\Delta_{\max}$ reveal the minimum and maximum difference between values after grey analysis, respectively. $\Delta_{0i}(k)$ demonstrates data value for *i*th response and *k*th test after grey analysis, and $\xi_i(k)$ is the grey relational coefficient. Each parameter in Eq.(7) can be calculated from Eqs. (8-10).

$$\Delta_{0i}(k) = \left\| X_0^*(k) - X_i^*(k) \right\| \quad (8)$$

$$\Delta_{\max} = \max\max \left\| X_0^*(k) - X_i^*(k) \right\| \quad (9)$$

$$\Delta_{\min} = \min\min \left\| X_0^*(k) - X_i^*(k) \right\| \quad (10)$$

Grey relational coefficient is the number between zero and one as stated by [37] and optimal grey coefficients are usually selected as average (0.5).

2.2.5. Grey relational grade

With the values computed for obtaining grey relational coefficient for each objective parameter, grey relational grade is calculated from Eq. (11) [38].

$$\gamma_i = \frac{1}{m}\sum_{i=1}^{m} \omega_i \xi_{ij} \quad (11)$$

$$\sum_{i=1}^{m} \omega_i = 1 \quad (12)$$

Where ω_i is the weight percent of a parameter, γ_i is the grey relational grade for the

*i*th experiment. The values of grey relational grade are listed in Table 5.

Both Table 5 and Fig. 3 show that the optimal condition occurs at simulation number 20. In this simulation, the grey relational grade is closer to one, so optimization suggests that the geometry for this experiment is the best for achieving the minimum required load and minimum inhomogeneity index of PEEQ.

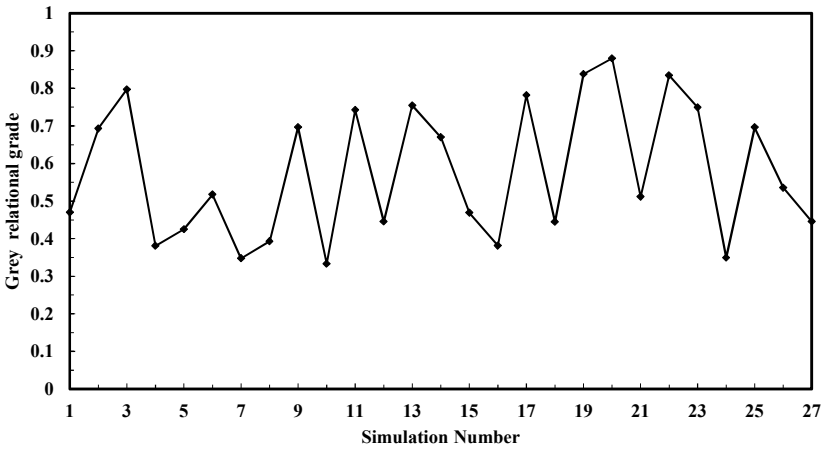

Fig 3. Graph of grey relational grade

2.2.6. Grey relational grade for each level

For each level, the grey relational grade is the average amount of grades in that level (Eqs. 13 and 14) [39-41].

$$\overline{A} = \frac{1}{k}\sum_{i=1}^{k}\gamma_i \quad (13)$$

$$k = \frac{m}{n} \quad (14)$$

where $\overline{A}$ is the grey relational grade for each level, k is a constant coefficient of equation, m is the number of tests, and n is level number. "Max – Min" in Table 6 shows the difference between maximum and minimum values of the grey relational grade for each level. The corresponding value reveals the sensitivity of objectives for the related parameter. Higher values indicate higher sensitivity and lower values specify lower sensitivity [39]. In all of the cases the values of "Max – Min" for ψ_2 are higher than that for ψ_1. This means that the objectives are more sensitive to ψ_2. Moreover, in the case of Φ_1=165 and for ψ_2, the maximum value of "Max – Min" (0.354) occurs. So, comparing other conditions, the objectives show the highest sensitivity in this case. Also, the minimum value of "Max – Min" (0.124) occurs for Φ_1=155 and ψ_1. So, varying of this parameter causes the least change of the objectives.

Table 6. Grey relational grade for each level

Parameters		Average grey relational grade by factor level			
		Level 1	Level 2	Level 3	Max–Min
Φ_1=145	ψ_1	0.653	0.441	0.479	0.212
	ψ_2	0.400	0.504	0.670	0.271
Φ_1=155	ψ_1	0.507	0.631	0.536	0.124
	ψ_2	0.490	0.731	0.453	0.278
Φ_1=165	ψ_1	0.743	0.644	0.559	0.184
	ψ_2	0.789	0.722	0.436	0.354

2.2.7. Grey relational graph

The graph of Table 6 is the grey relational graph. It indicates the graph of the gray relational grade for different levels. The steepness shows higher sensitivity and specifies the higher effect of that parameter. Fig. 4(a) reveals that in the case of Φ_1=145, the objectives are more sensitive to ψ_2 and changing this parameter causes more effect on two objectives. Fig. 4(b) and (c) show the same results. It is concluded that for all simulations, parameter ψ_2 has more effectiveness than parameter ψ_1. Furthermore, decreasing the amount of Φ_1 from 165 to 145 shows decreasing tendency of ψ_2, but does not show any significant trend for ψ_1.

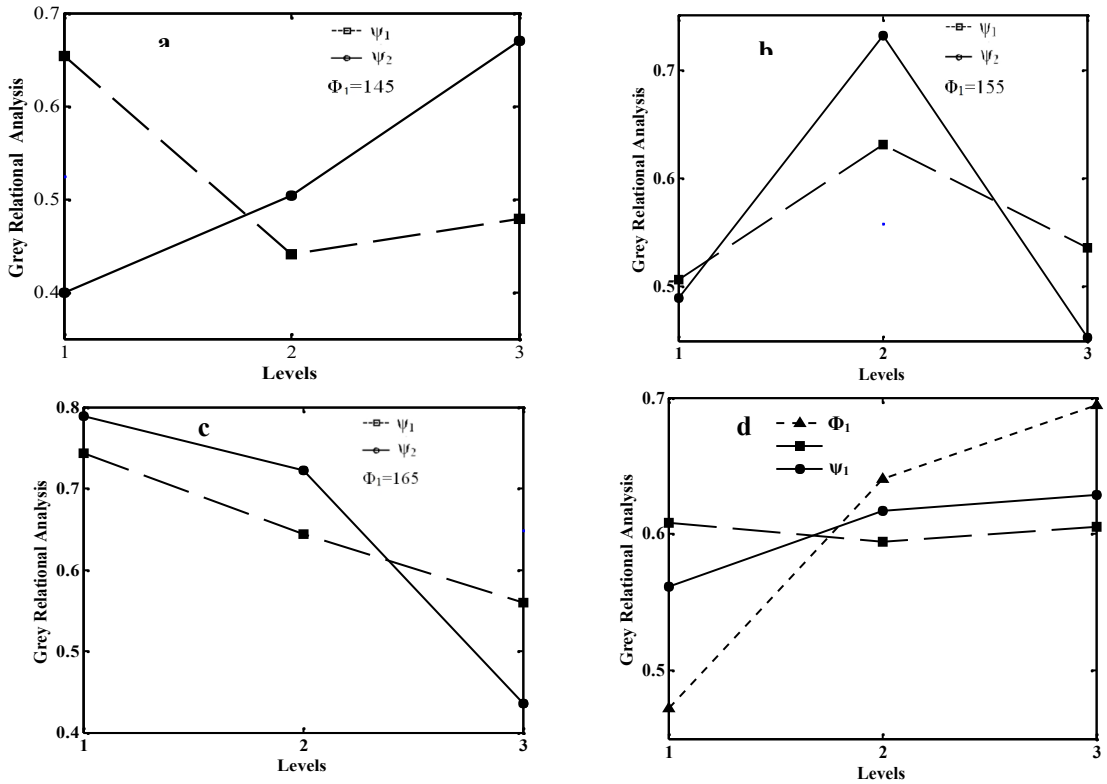

Fig 4. Grey relational graph: (a) Φ_1=145°, $\psi_1$and ψ_2 are variables, (b) Φ_1=155°, $\psi_1$and ψ_2 are variables, (c) Φ_1=165°, $\psi_1$and ψ_2 are variables and (d) Φ_1, $\psi_1$and ψ_2 are variables

2.2.8 Parameter effectiveness in optimum condition

The effectiveness of each parameter was calculated from Eq. (15)

$$\alpha_i = \left[\frac{N\overline{A}_{ij}}{\sum_{i=1}^{m} N\overline{A}_{ij}} \right] \times 100 \quad (15)$$

where, $N\overline{A}_{ij}$ is the difference between the maximum and a minimum amount of grey relational coefficient for each level and α_i denotes the parameter effectiveness in optimum condition. The calculated values for effectiveness in optimum condition for all parameters are listed in Table 7. It is inferred from Table 7 that in all three conditions for Φ_1, the effectiveness of ψ_2 is almost twice the effectiveness of ψ_1 (Fig. 5).

Table 7. Effectiveness of parameters in optimum condition

		Parameter effectiveness
Φ_1=145	ψ_1	43.911
	ψ_2	56.089
Φ_1=155	ψ_1	30.845
	ψ_2	69.155
Φ_1=165	ψ_1	34.188
	ψ_2	65.812

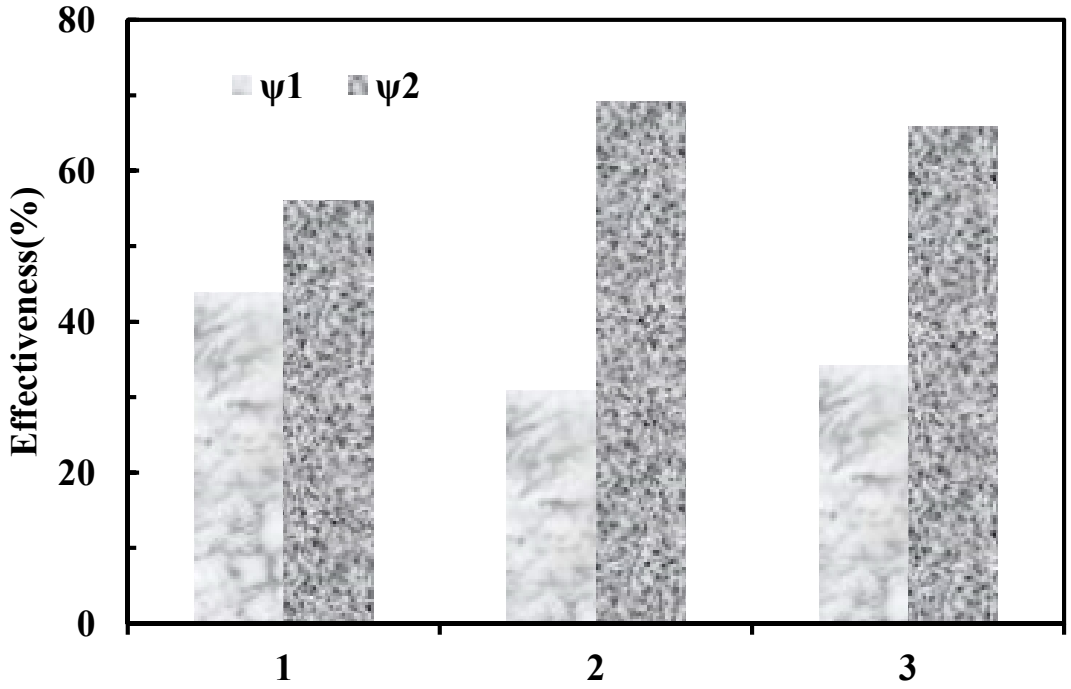

Fig 5. Graph of parameters effectiveness in optimum condition

$$N\overline{A}_{ij} = (\mathrm{Max}_{ij} - \mathrm{Min}_{ij}) \quad (16)$$

2.2.9. Parameter effectiveness on each objective

Any input parameter affects each objective parameter that can be calculated from Eqs. (17-20). The value of effectiveness shows the amount of objective dependence. The higher amount of effectiveness values shows more dependence of objective on the input parameter.

$$\overline{B} = \frac{1}{k}\sum_{i=1}^{k}\zeta_i \quad (17)$$

$$k = \frac{m}{n} \quad (18)$$

$$B_i = \left[\frac{N\overline{B}_{ij}}{\sum_{i=1}^{m} N\overline{B}_{ij}}\right] \times 100 \quad (19)$$

where $\overline{B}$ is the grey relational grade for each parameter, k is a constant coefficient of equation, m is the number of tests, and n is the level number.

B_i is the effectiveness percent of *ith* parameter for *jth* level and NB_{ij} is the value of Max-Min grey relational coefficient for each level. Table 8 lists the effectiveness values of the input parameters on the objective parameters. In the second and third cases of Φ_1 and when maximum required load is an objective, the effectiveness of ψ_2 is more than that of ψ_1. But in the first case (Φ_1=145), results show that the value of effectiveness for ψ_1 is higher. Also, by increasing the value of Φ_1, the effectiveness of ψ_1 reduces from 67.928% to 25.935% and as a result the influence of ψ_2 on objective rises from 32.072% to 74.065%. For another objective (the inhomogeneity index) it is inferred from Table 8 that for all cases, the effectiveness of ψ_2 is more than the effectiveness of ψ_1 and by increasing the value of Φ_1, there is not any distinct trend for parameters effectiveness.

Table 8. Parameters effectiveness on the objective parameters

		Maximum required load	Inhomogeneity index
Φ_1=145	ψ_1	67.928	21.775
	ψ_2	32.072	78.225
Φ_1=155	ψ_1	47.398	15.566
	ψ_2	52.602	84.434
Φ_1=165	ψ_1	25.935	46.172
	ψ_2	74.065	53.828

2.2.10 Graph of parameter effectiveness on each objective

The graph of effectiveness for all the parameters which were obtained in section 2.2.9 is depicted in Fig. 6. It is inferred that in almost all cases (except Φ_1=145 and maximum required load as the first objective parameter), the effectiveness of ψ_2 is higher than the effectiveness of ψ_1. Maximum and minimum value of effectiveness occurs when the Φ_1=155 and the inhomogeneity index was taken as the objective. In this situation the maximum and minimum value of effectiveness occurs for ψ_2 and ψ_1, respectively.

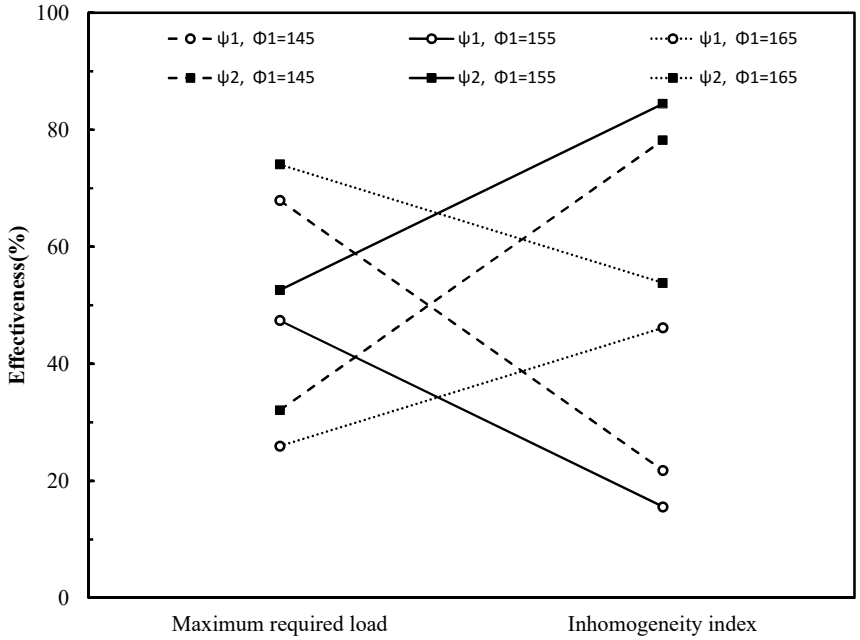

Fig 6. Graph of parameter effectiveness on each objective

3. Results and discussion

3.1. Finite element and experimental procedures

The deformed shape of the strip in both routes is illustrated in Fig. 7. There are some similarities between the results for PEEQ of both routes: 1) It is obvious that except for the front and end part of strips, three separate regions exist due to the first, second and third channel. Because of different deformation history the front and end part of the strips are not similar. 2) It is concluded that at the end of the process the strain is almost steady along the work-piece.

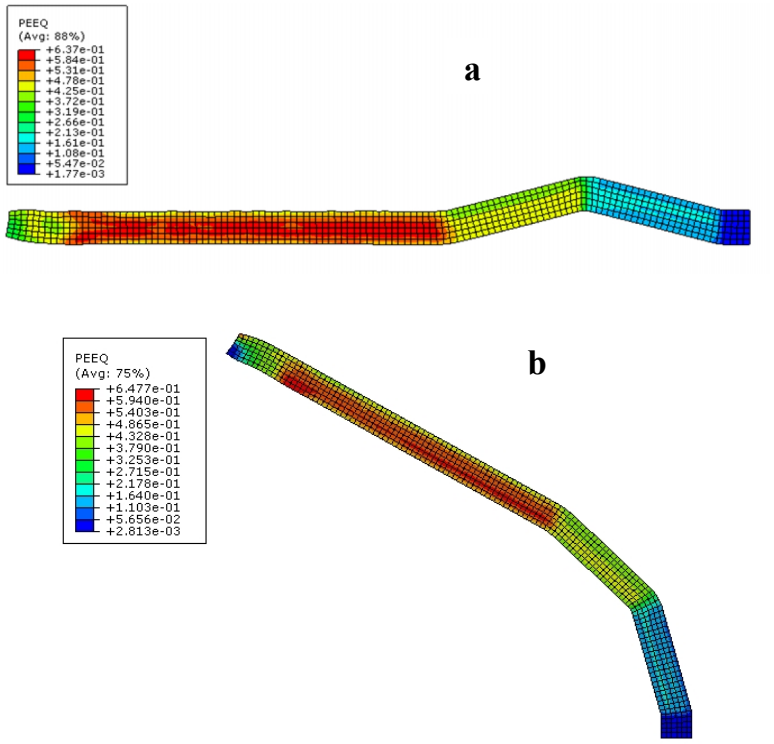

Fig 7.PEEQ results: (a) route C and (b) route A

Also, there are some dissimilarities between the routes. It is depicted that for each ECMAP pass, maximum PEEQ after the ECMAP will be ~ 0.64 and ~0.68 for route C & A, respectively. Moreover, at the end of the process the strain is steadier along the thickness of the work-piece for route C. For the ECMAPed strip, the amount of PEEQ is high at the middle of the strip and decreases toward the outer surfaces. So, PEEQ is at its minimum on the surfaces and maximum in the center of the strip, and this trend has symmetry from center to both top and bottom ends. However, it is different for route A. The values of PEEQ do not have any balance, and the maximum strains are generated in one side of strip.

From the simulation results, the values for PEEQ are obtained (Fig. 8). It is clear that for both routes the values of PEEQ are higher in the middle part of the specimen and it descends toward the outer surfaces of the strips. Moreover, although the amount of strain is greater in route A, the homogeneity is lower than route C.

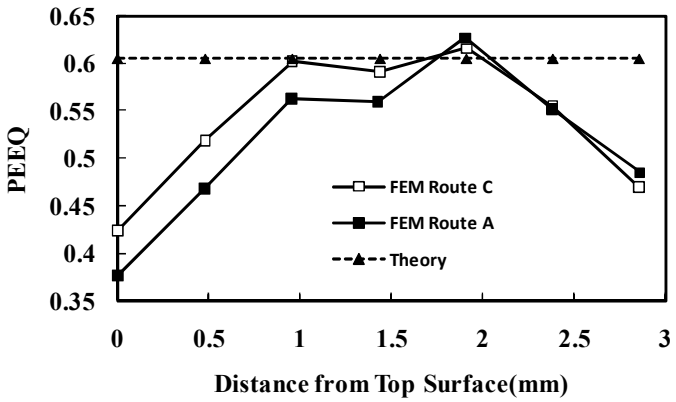

Fig 8. FEM and theory results for PEEQ

For validation of finite element results, the amount of PEEQ was achieved from analytical method, too [42]. Because of not considering friction and material properties, the analytical methods give constant lines. For both geometries used in this study Eq. (21) was employed.

$$\bar{\varepsilon}_T = \sum_{i=1}^{3}\left[\frac{2\cot(\varphi_i/2+\psi_i/2)+\psi_i\cos ec(\varphi_i/2+\psi_i/2)}{\sqrt{3}}\right] \quad (21)$$

The parameters Φ_1, Φ_2, $\psi_1$and ψ_2 were taken to be 165°, 150°, 15° and 30°, respectively. Fig. 8 depicts the theoretical result for PEEQ.

One of the main factors that indicate the higher potential to create more passes is higher homogeneity. With the aim of homogeneity survey and more comparison of FEM with experimental results the inhomogeneity index for PEEQ results was obtained from Eq. (22) [43].

$$C_i = \frac{\varepsilon_{\max}-\varepsilon_{\min}}{\varepsilon_{avg}} \quad (22)$$

Whereε_m ,ε_m and ε_a denote the maximum, minimum, and the average of PEEQ in the cross section plane, respectively.

The obtained values for inhomogeneity indexes are 0.356 and 0.482 for route C and route A respectively. This shows that comparing route A, the homogeneity is more in route C.

The other important factor in ECMAP is the required load of the process, which could be obtained from FEM. Fig. 9 depicts the force-displacement curve during the process for both routes. It is evident that the trend of the force-displacement curve varies in four different zones. The sharp change of the first zone occurs when the strip reaches the end of the first and beginning of the second channel. Once the strip starts moving in the second channel, the hydrostatic force increases noticeably and this occurrence leads to a rise in friction force and subsequently the required pressing force. After moving from the first channel, the identical incidences take place for deforming strip in the second and third channels. It means that when the strip reaches the end of each channel, due to the enhancement of friction force, the required force increases suddenly. It is evident that at the end of the third and beginning of the fourth channel, the force displacement curve reaches the top value due to strain hardening in previous channels, the maximum hydrostatic, and friction force. After this step, due to declining friction surface and consequently the friction force, the force displacement curve reduces smoothly.

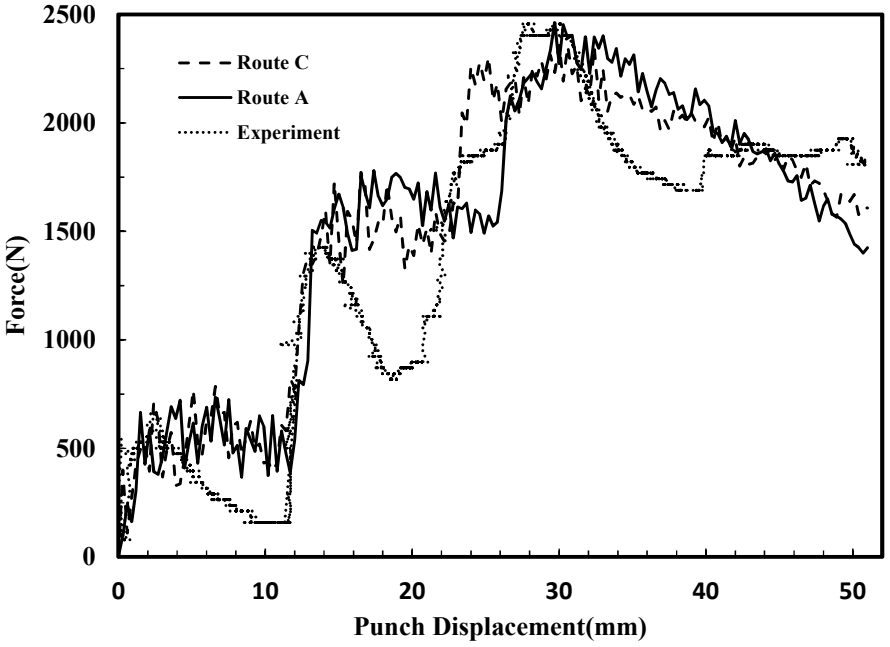

Fig 9. Force displacement curve for both routes

From simulation results, it is inferred that although PEEQ in route A is higher than that in route C, the homogeneity as a quality factor for route C is higher. Moreover, it is concluded that the required load for route C is lower than that in route A. So, route C was selected for more investigation and optimization.

From the strips obtained from route C, microhardness measurements were done on the three strips. Hardness measurements were done on seven points in the cross section starting from the top surface to the bottom for all pieces and average amount was exploited for each point (Fig. 10). It is concluded that for the ECMAPed specimens, the hardness values near the top and bottom surfaces are minimum while it increases toward the middle part of the strips. Also, the hardness measurements that were presented in Fig. 10 show good similarity with results of Fig. 8. The trend of microhardness values and PEEQ is similar, so simulation results have good conformity with experimental values.

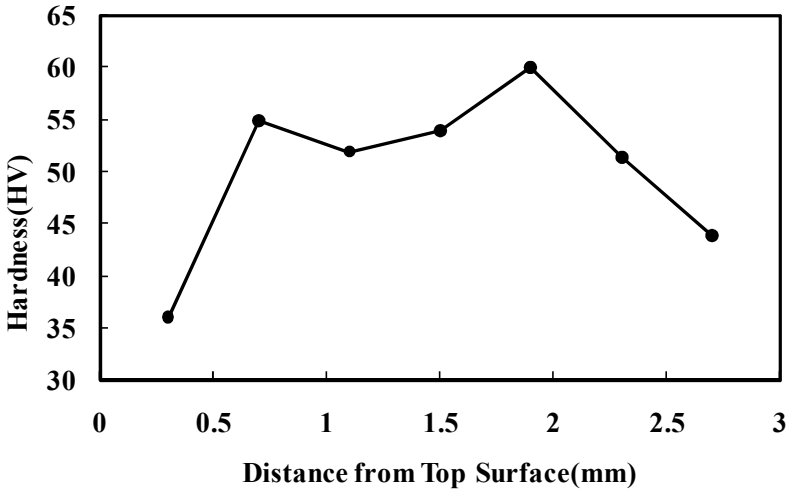

Fig 10. Hardness values from the cross section of specimen

Also, the inhomogeneity index for hardness results was obtained from Eq. (23), [43].

$$H_i = \frac{H_{\max} - H_{\min}}{H_{avg}} \quad (23)$$

Where H_m , H_m and H_a denote the maximum, minimum, and average of hardness in the cross section plane, respectively. The obtained values for the inhomogeneity index of hardness is $H_i = 0.477$ that is close to the value of inhomogeneity index for PEEQ of route C.

In the next section, Grey relational analysis is used as the optimization method. Geometrical parameters were taken as input variables and both inhomogeneity index and maximum required load were taken as objectives.

3.2. Optimization

Die corner angles (ψ_i) are not constant and for each value of die channel angle, different amount of die corner angles can be selected. Effects of various die corner angles in three cases of Φ_1 were investigated and the results are illustrated in Table 6 and Fig. 4. It was concluded that in all three cases of Φ_1, the influence of ψ_2 is greater than ψ_1. Also, it was inferred from Fig. 4(d) that Φ_1 is the most effective parameter when all geometrical parameters are considered as input variables. The effectiveness of both ψ_1 and ψ_2 on all objective parameters is shown in Fig. 5 and Table 7. It is concluded that the maximum effectiveness of ψ_2 on the objective parameters is 69.155% and related to 155° for Φ_1. Also, the highest influence of ψ_1 on the objectives is 43.911% and belongs to 145° for Φ_1.

The effectiveness of all input parameters on each output parameter is shown in Table 8 and Fig. 6. It was concluded that strain inhomogeneity index was influenced mostly by angle ψ_2 when the amount of Φ_1 equals to 155°. Also, when Φ_1 equals to 165°, the most effective angle is ψ_2 when the required load is taken as objective.

Table 9. Best and weakest conditions for each Φ_1

	Best conditions		weakest conditions	
	ψ_1	ψ_2	ψ_1	ψ_2
Φ_1=145	0	70	35	0
Φ_1=155	25	25	0	0
Φ_1=165	0	15	7.5	30

Table 10. Optimum condition for all simulations

Optimum conditions	
Parameters	Optimal values
Φ_1	165
ψ_1	0
ψ_2	15

4. Conclusions

To do a complete study on available routes in the production of UFG Al1050 strips, two main routes A and C were investigated by FEM and compared with each other. Maximum strain, maximum required force and strain inhomogeneity index in both routes were evaluated. The obtained results of FEM were verified by both theoretical calculations and experimental tests. Furthermore, it is inferred that although maximum value of PEEQ in route A is higher than that in route C, the homogeneity as a quality factor for route C is higher. Moreover, it is concluded that the required load for route C is lower than that for route A. So, route C was selected for more investigation and optimization. Grey relational analysis was used as the optimization method. For all input and output parameters, optimization was done and optimum values of input parameters and also the effectiveness of each parameter was obtained. The optimum condition occurs when Φ_1, ψ_1 and ψ_2 are 165°, 0° and 15°, respectively and for specific value of Φ_1, the effectiveness of ψ_2 is almost twice the effectiveness of ψ_1.

References

[1] R.Z. Valiev, T.G. Langdon, "Principles of equal-channel angular pressing as a processing tool for grain refinement", Progress in Materials Science, Vol. 51, No. 7, 2006, pp. 881-981.

[2] P. Bergwerf, "Equall channel angullar pressing of high carbon steel", Master Thesis, Delf

University of Technology, Vol. No. 12 March 2007, pp.

[3] G. Faraji, M. Ebrahimi, A. Bushroa, "Ultrasonic assisted tubular channel angular pressing process", Materials Science and Engineering: A, Vol. 599, No. 2014, pp. 10-15.

[4] M. Furukawa, Z. Horita, M. Nemoto, R.Z. Valiev, T.G. Langdon, "Microstructural characteristics of an ultrafine grain metal processed with equal-channel angular pressing", Materials characterization, Vol. 37, No. 5, 1996, pp. 277-283.

[5] R. Jahadi, M. Sedighi, H. Jahed, "Ecap effect on the micro-structure and mechanical properties of am30 magnesium alloy", Materials Science and Engineering: A, Vol. 593, No. 2014, pp. 178-184.

[6] S. Rusz, L. Cizek, M. Salajka, S. Tylsar, J. Kedron, V. Michenka, T. Donic, E. Hadasik, M. Klos, "Ultrafine grain refinement of almn1cu and az 31 alloys by spd process", Archives of Metallurgy and Materials, Vol. 59, No. 1, 2014, pp. 359-364.

[7] V. Segal, "Materials processing by simple shear", Materials Science and Engineering: A, Vol. 197, No. 2, 1995, pp. 157-164.

[8] Y. Yuan, A. Ma, J. Jiang, Y. Sun, F. Lu, L. Zhang, D. Song, "Mechanical properties and precipitate behavior of mg–9al–1zn alloy processed by equal-channel angular pressing and aging", Journal of Alloys and Compounds, Vol. 594, No. 2014, pp. 182-188.

[9] G. Deng, C. Lu, L. Su, A.K. Tieu, J. Li, M. Liu, H. Zhu, X. Liu, "Influence of outer corner angle (oca) on the plastic deformation and texture evolution in equal channel angular pressing", Computational Materials Science, Vol. 81, No. 2014, pp. 79-88.

[10] H.S. Kim, M.H. Seo, S.I. Hong, "On the die corner gap formation in equal channel angular pressing", Materials Science and Engineering: A, Vol. 291, No. 1, 2000, pp. 86-90.

[11] S. Li, X. Li, L. Yang, "Role of strain path change in grain refinement by severe plastic deformation: A case study of equal channel angular extrusion", Acta Materialia, Vol. 61, No. 12, 2013, pp. 4398-4413.

[12] P. Prangnell, C. Harris, S. Roberts, "Finite element modelling of equal channel angular extrusion", Scripta Materialia, Vol. 37, No. 7, 1997, pp. 983-989.

[13] F. Salimyanfard, M.R. Toroghinejad, F. Ashrafizadeh, M. Hoseini, J.A. Szpunar, "Investigation of texture and mechanical properties of copper processed by new route

of equal channel angular pressing", Materials & Design, Vol. 44, No. 2013, pp. 374-381.
[14] S. Semiatin, D. Delo, E. Shell, "The effect of material properties and tooling design on deformation and fracture during equal channel angular extrusion", Acta Materialia, Vol. 48, No. 8, 2000, pp. 1841-1851.
[15] S. Arab, A. Akbarzadeh, "The effect of equal channel angular pressing process on the microstructure of az31 mg alloy strip shaped specimens", Journal of Magnesium and Alloys, Vol. 1, No. 2, 2013, pp. 145-149.
[16] J.Y. Park, D.N. Lee, "Deformation and annealing textures of equal-channel angular pressed 1050 al alloy strips", Materials Science and Engineering: A, Vol. 497, No. 1, 2008, pp. 395-407.
[17] K. Nakashima, Z. Horita, M. Nemoto, T.G. Langdon, "Development of a multi-pass facility for equal-channel angular pressing to high total strains", Materials Science and Engineering: A, Vol. 281, No. 1, 2000, pp. 82-87.
[18] H.S. Kim, "Finite element analysis of deformation behaviour of metals during equal channel multi-angular pressing", Materials Science and Engineering: A, Vol. 328, No. 1, 2002, pp. 317-323.
[19] J. Jung, S.C. Yoon, H.-J. Jun, H.S. Kim, "Finite element analysis of deformation homogeneity during continuous and batch type equal channel angular pressing", Journal of materials engineering and performance, Vol. 22, No. 11, 2013, pp. 3222-3227.
[20] G. Faraji, A. Babaei, M.M. Mashhadi, K. Abrinia, "Parallel tubular channel angular pressing (ptcap) as a new severe plastic deformation method for cylindrical tubes", Materials Letters, Vol. 77, No. 2012, pp. 82-85.
[21] G. Faraji, M. Mousavi Mashhadia, "Plastic deformation analysis in parallel tubular channel angular pressing (ptcap)", Journal of Advanced Materials and Processing, Vol. 1, No. 4, 2013, pp. 23-32.
[22] G. Faraji, M. Mashhadi, K. Abrinia, H. Kim, "Deformation behavior in the tubular channel angular pressing (tcap) as a noble spd method for cylindrical tubes", Applied Physics A, Vol. 107, No. 4, 2012, pp. 819-827.
[23] G. Faraji, M. Mashhadi, A. Dizadji, M. Hamdi, "A numerical and experimental study on tubular channel angular pressing (tcap) process", Journal of mechanical science and technology, Vol. 26, No. 11, 2012, pp. 3463-3468.
[24] G. Faraji, P. Yavari, S. Aghdamifar, M.M. Mashhadi, "Mechanical and microstructural properties of ultra-fine grained az91 magnesium alloy tubes processed via multi pass tubular channel angular pressing (tcap)", Journal of Materials Science & Technology, Vol. 30, No. 2, 2014, pp. 134-138.
[25] H.-j. Hu, D.-f. Zhang, F.-s. Pan, "Die structure optimization of equal channel angular extrusion for az31 magnesium alloy based on finite element method", Transactions of Nonferrous Metals Society of China, Vol. 20, No. 2, 2010, pp. 259-266.
[26] E. López-Chipres, E. García-Sanchez, E. Ortiz-Cuellar, M. Hernandez-Rodriguez, R. Colás, "Optimization of the severe plastic deformation processes for the grain refinement of al6060 alloy using 3d fem analysis", Journal of Materials Engineering and Performance, Vol. No. 2010, pp. 1-7.
[27] A. Nagasekhar, Y. Tick-Hon, "Optimal tool angles for equal channel angular extrusion of strain hardening materials by finite element analysis", Computational Materials Science, Vol. 30, No. 3, 2004, pp. 489-495.
[28] T. Suo, Y. Li, Q. Deng, Y. Liu, "Optimal pressing route for continued equal channel angular pressing by finite element analysis", Materials Science and Engineering: A, Vol. 466, No. 1, 2007, pp. 166-171.
[29] S. Xu, G. Zhao, X. Ma, G. Ren, "Finite element analysis and optimization of equal channel angular pressing for producing ultra-fine grained materials", Journal of Materials Processing Technology, Vol. 184, No. 1, 2007, pp. 209-216.
[30] C. Wang, F. Li, H. Lu, Z. Yuan, B. Chen, "Optimization of structural parameters for elliptical cross-section spiral equal-channel extrusion dies based on grey theory", Chinese Journal of Aeronautics, Vol. 26, No. 1, 2013, pp. 209-216.
[31] F. Fereshteh-Saniee, M. Asgari, M. Barati, S.M. Pezeshki, "Effects of die geometry on non-equal channel lateral extrusion (necle) of az80 magnesium alloy", Transactions of

Nonferrous Metals Society of China, Vol. 24, No. 10, 2014, pp. 3274-3284.

[32] A. Shokuhfar, O. Nejadseyfi, "The influence of friction on the processing of ultrafine-grained/nanostructured materials by equal-channel angular pressing", Journal of materials engineering and performance, Vol. 23, No. 3, 2014, pp. 1038-1048.

[33] U. Çaydaş, A. Hasçalık, "Use of the grey relational analysis to determine optimum laser cutting parameters with multi-performance characteristics", Optics & laser technology, Vol. 40, No. 7, 2008, pp. 987-994.

[34] D.K. Panda, "Modelling and optimization of multiple process attributes of electrodischarge machining process by using a new hybrid approach of neuro–grey modeling", Materials and Manufacturing Processes, Vol. 25, No. 6, 2010, pp. 450-461.

[35] S. Khalilpourazary, P. Kashtiban, N. Payam, "Optimization of turning operation of st37 steel using grey relational analysis", Vol. No. 2014, pp.

[36] C.-J. Tzeng, Y.-H. Lin, Y.-K. Yang, M.-C. Jeng, "Optimization of turning operations with multiple performance characteristics using the taguchi method and grey relational analysis", Journal of materials processing technology, Vol. 209, No. 6, 2009, pp. 2753-2759.

[37]K. Palanikumar, B. Latha, V. Senthilkumar, J.P. Davim, "Analysis on drilling of glass fiber–reinforced polymer (gfrp) composites using grey relational analysis", Materials and Manufacturing Processes, Vol. 27, No. 3, 2012, pp. 297-305.

[38] J.A. Barrios, A. Cavazos, L. Leduc, J. Ramirez, "Fuzzy and fuzzy grey-box modelling for entry temperature prediction in a hot strip mill", Materials and Manufacturing Processes, Vol. 26, No. 1, 2011, pp. 66-77.

[39] J. Kopac, P. Krajnik, "Robust design of flank milling parameters based on grey-taguchi method", Journal of Materials Processing Technology, Vol. 191, No. 1, 2007, pp. 400-403.

[40] H. Lu, C. Chang, N. Hwang, C. Chung, "Grey relational analysis coupled with principal component analysis for optimization design of the cutting parameters in high-speed end milling", Journal of materials processing technology, Vol. 209, No. 8, 2009, pp. 3808-3817.

[41] L.K. Pan, C.C. Wang, S.L. Wei, H.F. Sher, "Optimizing multiple quality characteristics via taguchi method-based grey analysis", Journal of Materials Processing Technology, Vol. 182, No. 1, 2007, pp. 107-116.

[42] Y. Iwahashi, Z. Horita, M. Nemoto, T.G. Langdon, "An investigation of microstructural evolution during equal-channel angular pressing", Acta Materialia, Vol. 45, No. 11, 1997, pp. 4733-4741.

[43] N. El Mahallawy, F.A. Shehata, M.A. El Hameed, M.I.A. El Aal, H.S. Kim, "3d fem simulations for the homogeneity of plastic deformation in al–cu alloys during ecap", Materials Science and Engineering: A, Vol. 527, No. 6, 2010, pp. 1404-1410.